



Spin transition of Fe³⁺ in Al-bearing phase D: An alternative explanation for small-scale seismic scatterers in the mid-lower mantle



Yun-Yuan Chang^{a,*}, Steven D. Jacobsen^a, Jung-Fu Lin^b, Craig R. Bina^a,
Sylvia-Monique Thomas^{a,1}, Junjie Wu^b, Guoyin Shen^c, Yuming Xiao^c, Paul Chow^c,
Daniel J. Frost^d, Catherine A. McCammon^d, Przemyslaw Dera^e

^a Department of Earth and Planetary Sciences, Northwestern University, Evanston, IL 60208, USA

^b Department of Geological Sciences, Jackson School of Geosciences, The University of Texas at Austin, Austin, TX 78712, USA

^c HPCAT, Geophysical Laboratory, Carnegie Institution of Washington, Argonne, IL, USA

^d Bayerisches Geoinstitut, University of Bayreuth, D-95440 Bayreuth, Germany

^e GeoSoilEnviroCARS, University of Chicago, Argonne National Laboratory, Argonne, IL 60439, USA

ARTICLE INFO

Article history:

Received 15 January 2013

Received in revised form 26 July 2013

Accepted 22 August 2013

Available online 24 September 2013

Editor: L. Stixrude

Keywords:

dense hydrous magnesium silicate

phase D

spin transition

lower mantle

seismic scatterers

ABSTRACT

Among dense-hydrous magnesium silicates potentially transporting H₂O into Earth's deep interior, phase D (MgSi₂H₂O₆) exhibits the highest *P*–*T* stability range, extending into the lower mantle along cold slab geotherms. We have studied the compressibility and spin state of Fe in Al-bearing phase D up to 90 GPa using synchrotron X-ray diffraction and X-ray emission spectroscopy. Fe–Al-bearing phase D was synthesized at 25 GPa and 1400 °C with approximate composition MgSi_{1.5}Fe_{0.15}Al_{0.32}H_{2.6}O₆, where nearly all of the Fe is ferric (Fe³⁺). Analysis of Fe-Kβ emission spectra reveals a gradual, pressure-induced high-spin (HS) to low-spin (LS) transition of Fe³⁺ extending from 40 to 65 GPa. The fitted equation of state for high-spin Fe–Al-bearing phase D results in a bulk modulus $K_{T0} = 147(2)$ GPa with pressure derivative $K' = 6.3(3)$. An equation of state over the entire pressure range was calculated using the observed variation in low-spin fraction with pressure and a low-spin bulk modulus of $K_{T0} = 253(30)$ GPa, derived from the data above 65 GPa. Pronounced softening in the bulk modulus occurs during the spin transition, reaching a minimum at 50 GPa (~1500 km) where the bulk modulus of Fe–Al phase D is about 35% lower than Fe–Al-bearing silicate perovskite. Recovery of the bulk modulus at 50–65 GPa results in a structure that has a similar incompressibility as silicate perovskite above 65 GPa. Similarly, the bulk sound velocity of Fe–Al phase D reaches a minimum at ~50 GPa, being about 10% slower than silicate perovskite. The potential association of Fe–Al phase D with subducted slabs entering the lower mantle, along with its elastic properties through the Fe³⁺ spin transition predicted at 1200–1800 km, suggests that phase D may provide an alternative explanation for small-scale mid-lower mantle seismic scatterers and supports the presence of deeply recycled sediments in the lower mantle.

© 2013 Elsevier B.V. All rights reserved.

1. Introduction

Subducted oceanic crust can carry kilometer-thick packages of Fe- and Al-rich pelitic sediments into the upper mantle at convergent margins where the average continental shale contains 5–8 wt.% Fe₂O₃ + FeO and 15–25 wt.% Al₂O₃ (e.g. Plank and Langmuir, 1998; Poli and Schmidt, 2002). Dehydration reactions of serpentinite-group minerals can produce a number of different dense hydrous magnesium silicates (DHMS) in the MgO–SiO₂–H₂O system along cold subduction geotherms (e.g. Angel et al., 2001;

Irfune et al., 1998; Ohtani et al., 2001; Ringwood and Major, 1967; Yamamoto and Akimoto, 1977). Fluids from dehydrating crust and sediments also interact with downgoing entrained peridotite from the overlying mantle wedge (Kawakatsu and Watada, 2007). Thus, the contribution of chemical components from subducted sediments (H₂O, Fe₂O₃ and Al₂O₃) may influence phase relations and physical properties of DHMS in the peridotite system and is relevant to understanding the fate of subducted sediments in the mantle and Earth's deep water cycle.

DHMS occurring along the forsterite–brucite join (Fo, Mg₂SiO₄; Br, Mg(OH₂)) include phase A (2Fo + 3Br, 12 wt.% H₂O), OH-chondrodite (2Fo + 1Br, 5 wt.% H₂O), and OH-clinohumite (4Fo + 1Br, 3 wt.% H₂O), which are commonly found in dehydration experiments of serpentine below 15 GPa and 1200 °C (e.g. Luth, 1995; Stalder and Ulmer, 2001). At higher pressures of 15–30 GPa,

* Corresponding author.

E-mail address: ychang@earth.northwestern.edu (Y.-Y. Chang).

¹ Now at: Department of Geoscience, University of Las Vegas, Las Vegas, NV 89154, USA.

phase E (2Br + 1SiO₂, 10 wt.% H₂O), superhydrous phase B (3Fo + 2Br + 2MgO, 3 wt.% H₂O), and phase D (1Br + 2SiO₂, 10 wt.% H₂O) are the stable DHMS formed from serpentine-group minerals (e.g. Frost and Fei, 1998; Irifune et al., 1998; Ohtani et al., 2001; Shieh et al., 2000). Phase D is the highest-pressure phase among DHMS and has a dense structure ($\rho_0 = 3.51$ g/cm³) with Si in six-fold coordination similar to silicate perovskite. Phase D has therefore been considered a candidate phase for transport of H₂O into the lower mantle.

A path to phase D in the mantle requires breakdown of serpentine below the critical condition of $\sim 600^\circ\text{C}$ at 5 GPa, forming phase A plus enstatite (En, MgSiO₃) and fluid H₂O (e.g. Ulmer and Trommsdorff, 1995). Along cold slab geotherms, the phase A plus En assemblage is stable to ~ 12 GPa, where it will form phase E plus wadsleyite and further transform to superhydrous phase B plus stishovite above ~ 15 GPa (Litasov and Ohtani, 2003; Komabayshi and Omori, 2006). If temperatures remain below $\sim 1200^\circ\text{C}$, phase D will form at pressures above 15–18 GPa (e.g. Irifune et al., 1998; Kawamoto, 2004; Komabayshi and Omori, 2006). In other bulk compositions, phase D has been synthesized at temperatures as high as 1400°C at 25 GPa (Frost and Fei, 1998; Saikia et al., 2009). The upper stability limit of pure-Mg phase D was found to be ~ 44 GPa at 1200°C in laser-heated diamond-anvil cell experiments of serpentinite bulk compositions (Shieh et al., 1998). Litasov et al. (2008) measured the thermal equation of state of Al–Fe-bearing phase D up to 20 GPa and 1273 K; however, the upper stability limit of Al–Fe-bearing phase D has not been determined in comparison with pure-Mg phase D.

Phase D has a trigonal structure with space group *P31m*, composed of alternating layers of MgO₆ and SiO₆ octahedra along the *c*-axis (Yang et al., 1997). The ideal chemical formula of phase D is MgSi₂H₂O₆, although the observed stoichiometry varies in H-content from 2.2 to 3.6 H per formula unit and with Mg/Si ratios from 0.2 to 0.7 (e.g. Boffa Ballaran et al., 2010; Frost and Fei, 1999; Yang et al., 1997). The Mg–Si octahedral framework of the phase D structure contributes to its relatively high density and extended stability field among other DHMS, despite consisting of nearly 10% H₂O by weight.

Symmetrization of the hydrogen bonds in phase D was predicted to occur at ~ 40 GPa in a first-principles study (Tsuchiya et al., 2005). Symmetric hydrogen bonds result from a single and symmetric potential well for hydrogen, mid-way between the oxygen pair of a hydrogen bond. In phase D, modified oxygen–oxygen interatomic potentials due to symmetric hydrogen bonding could increase its bulk modulus by $\sim 20\%$ and make the *c*-axis more incompressible (Tsuchiya et al., 2005). Previous studies have shown a change in the pressure-dependence of the *c/a* axial ratio of both pure-Mg and Fe-bearing phase D at pressures of ~ 15 GPa (Litasov et al., 2008), at ~ 20 GPa (Frost and Fei, 1999), at 25–30 GPa (Litasov et al., 2007), and at ~ 40 GPa (Shinmei et al., 2008; Hushur et al., 2011). There has been some speculation that the observed changes in *c/a* may result from symmetrization of the hydrogen bonds. However, a high-pressure FTIR study of phase D by Shieh et al. (2009) up to 42 GPa shows no major changes in the O–H stretching region attributable to hydrogen-bond symmetrization, suggesting that the observed changes in compression mechanism above ~ 40 GPa are unrelated to changes in hydrogen bonding. Possible symmetrization of the hydrogen bonding in phase D requires further investigation.

The isothermal bulk modulus (K_{T0}) of pure-Mg phase D has been determined experimentally in static compression experiments with results ranging from 130 to 168 GPa (Frost and Fei, 1999; Shinmei et al., 2008; Hushur et al., 2011). The highest pressure reached in previous static compression studies was ~ 56 GPa by Hushur et al. (2011), who observed a slight discontinuity in the volume–compression curve at 40 GPa, coincident with the pres-

sure predicted for hydrogen-bond symmetrization by Tsuchiya et al. (2005). Brillouin scattering measurements of the adiabatic bulk modulus (K_{S0}) of two different pure-Mg samples give a value of 175(15) GPa for the composition Mg_{1.02}Si_{1.71}H_{3.12}O₆ (Liu et al., 2004) and 155(3) GPa for Mg_{1.1}Si_{1.9}H_{2.4}O₆ (Rosa et al., 2012). Variable Mg/Si ratios and variable water content may be contributing to differences in measured bulk moduli of pure-Mg phase D, although no systematic trend between Mg/Si or H-content and *K* is observed in the literature data. Fe–Al-bearing phase D was studied by Litasov et al. (2007) showing a bulk modulus of 137(3) GPa for a sample of composition Mg_{0.89}Fe_{0.14}Al_{0.25}Si_{1.56}H_{2.93}O₆. Litasov et al. (2008) reported a bulk modulus of 141(3) GPa for phase D with composition Mg_{0.99}Fe_{0.12}Al_{0.09}Si_{1.75}H_{2.51}O₆. The elastic properties of phase D with composition Mg_{1.0}Fe_{0.11}Al_{0.03}Si_{1.9}H_{2.5}O₆ were studied using Brillouin scattering by Rosa et al. (2012), who reported a bulk modulus of 158(4) GPa.

An electronic spin transition of Fe from high spin (HS) to low spin (LS) has been documented in a number of Fe-bearing mantle minerals, including ferropericlase-(Mg,Fe)O (e.g. Badro et al., 2003; Lin et al., 2005, 2007; Speziale et al., 2005; Tsuchiya et al., 2006) and silicate perovskite-(Mg,Fe)SiO₃ (e.g. Badro et al., 2004; Catalli et al., 2011; Grocholski et al., 2009; Hsu et al., 2012; Jackson et al., 2005; Li et al., 2004; Lin et al., 2012). For reviews of Fe spin transitions in mantle minerals, see Li (2007) and Lin and Tsuchiya (2008). In (Mg,Fe)O, where the octahedral site hosts Fe²⁺, the spin transition begins to occur at 40–50 GPa (e.g. Lin and Tsuchiya, 2008). In silicate perovskite, Fe²⁺ and Fe³⁺ coexist on different sites and both may have multiple spin states. Fe³⁺ occupies both the A site and B sites of the ABO₃-perovskite structure, whereas Fe²⁺ occurs dominantly on the A site (e.g. Lin et al., 2012). In Al-bearing compositions, the Fe³⁺/ΣFe ratio and Fe³⁺ site occupancies are affected by the amount of aluminum (McCammon, 1997; Frost et al., 2004; Vanpeteghem et al., 2006; Hsu et al., 2012), making interpretation of HS–LS transitions of Fe in silicate perovskite considerably more complicated than in (Mg,Fe)O. The potentially high Al-content of phase D may influence the amount of Fe³⁺ in the structure, as has been shown in silicate perovskite (Frost et al., 2004; Saikia et al., 2009). The phase D sample in this study provides the opportunity to study the high-pressure spin-states of Fe³⁺ isolated on an octahedral site.

Pressure-induced spin transitions of Fe in (Mg,Fe)O and silicate perovskite are known to influence their elastic properties (e.g. Catalli et al., 2010; Crowhurst et al., 2008; Hsu et al., 2011; Mao et al., 2011; Marquardt et al., 2009; Speziale et al., 2007; Wentzcovitch et al., 2009), although the evolution of low-spin state fraction (*n*) with pressure, i.e. *n*(*P*) for different Fe valences (2+, 3+) on different sites remain difficult to isolate (Lin et al., 2012). The maximum pressure of previous studies on Fe–Al-bearing phase D is ~ 30 GPa, and therefore a potential electronic spin transition of Fe in phase D has not been investigated.

Here we report a spin transition of Fe in dense hydrous magnesium silicate phase D, a potential carrier of H₂O into the lower mantle. Using synchrotron X-ray emission spectroscopy in conjunction with X-ray diffraction up to ~ 90 GPa, we have determined the equation of state and identified a spin transition of Fe³⁺ on the octahedral site in phase D with composition MgSi_{1.5}Fe_{0.15}³⁺Al_{0.3}H_{2.6}O₆. This composition facilitates a study of the spin-transition character of Fe³⁺ isolated on the octahedral site of the structure. We observed a gradual HS to LS transition occurring between ~ 40 and 65 GPa, which results in a significant softening of the bulk modulus through the transition followed by recovery to values comparable to silicate perovskite in the lower mantle. The results are used to discuss phase D as a possible alternative explanation for small-scale seismic scatterers in the mid-lower mantle.

Table 1
Electron microprobe analysis of phase D from run S3602.

Oxide	Probe spot 1 (wt.%)	Probe spot 2 (wt.%)	Cation	Approx. apfu [*]
SiO ₂	50.94	49.77	Si	1.5
MgO	21.85	21.66	Mg	1.0
FeO	5.96	6.17	Fe	0.15
Al ₂ O ₃	8.77	9.01	Al	0.32
H ₂ O [†]	12.48	13.39	H	2.6
Total	100.0	100.0		

^{*} Atoms per formula unit, normalized to six oxygen atoms.

[†] H₂O wt.% calculated by difference to bring \sum wt.% = 100.

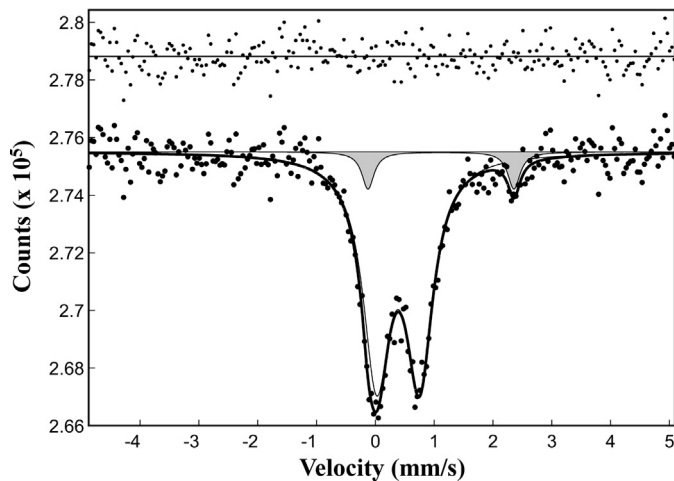


Fig. 1. Room temperature Mössbauer spectrum of Fe–Al phase D from run S3602, where the doublets assigned to Fe³⁺ and Fe²⁺ are unshaded and shaded grey, respectively. The relative abundance of different species is roughly equal to their relative areas, showing that nearly all of the iron is Fe³⁺. The residual is plotted above the spectrum.

2. Experimental methods

2.1. Sample synthesis and characterization

Phase D was synthesized in a multi-anvil press at 1400 °C and 25 GPa from starting materials of 34% Mg(OH)₂, 12% Al(OH)₃, 16% Fe₂O₃ and 38% SiO₂ by weight in run S6302 of Saikia et al. (2009). The mixture was heated for 60 min in a Pt capsule, resulting in mostly phase D with crystals ranging in size from 50 to 100 μm along with one very large single crystal of silicate perovskite measuring ~300 μm in size. Electron microprobe analyses are presented in Table 1, resulting in approximate composition MgSi_{1.5}Fe_{0.15}³⁺Al_{0.32}H_{2.6}O₆. A Mössbauer spectrum collected using a ⁵⁷Co in Rh point source in transmission geometry with a 200 μm beam size indicates that nearly all of the iron is ferric, with Fe³⁺/∑Fe = 0.93(3) (Fig. 1). From the Mössbauer spectrum of Fe³⁺ in phase D, we obtain a quadrupole splitting (QS) of 0.73(2) mm/s and isomer shift (IS) of 0.38(2) mm/s (relative to α-Fe), which is consistent with literature values for octahedral Fe³⁺ (e.g., Gütlich et al., 2011). Single-crystal X-ray diffraction measurements of the lattice parameters gives $a = 4.7964(1)$ Å, $c = 4.3224(4)$ Å, and $V = 86.116(7)$ Å³, resulting in a calculated density of $\rho_0 = 3.51(1)$ g/cm³.

2.2. High-pressure X-ray emission spectroscopy

High-pressure X-ray Fe-Kβ emission experiments were performed on the 16-IDD beamline (HPCAT) at the Advanced Photon Source (APS) using an incident beam energy tuned to 11.3 keV. Single crystals of phase D were double-side polished into plates

measuring about 50 μm across and 20 μm in thickness. Two XES runs were made in diamond-anvil cells using a heavy mineral oil pressure medium (EMD Chemicals Inc.; CAS# 8012-95-1). The first cell was fitted with 300 μm culet diamond anvils and a Be gasket. An annealed ruby sphere was used as the pressure calibrant (Mao et al., 1986) and experiments in this first run were carried out up to 60 GPa. In order to reach ~95 GPa, a second diamond-anvil cell was prepared with 200 μm culets, and a cubic boron-nitride (cBN) insert was made to strengthen the Be gasket (Lin et al., 2008). XES spectra were collected at ambient conditions using the same experimental setup as the high-pressure spectra. An XES spectrum of hematite was collected as Fe high-spin state standard, and a spectrum of ferropericlase-(Mg_{0.75}Fe_{0.25}) at 90 GPa was collected as Fe low-spin standard (Mao et al., 2011).

2.3. X-ray diffraction

Two compression experiments were conducted using synchrotron X-ray diffraction at sector 16 (HPCAT) at the APS. In run#1, a diamond-anvil cell with 200 μm culets was prepared with a Re gasket. A tungsten-carbide seat with 1-mm opening was used on the side of the X-ray source, and a cBN seat on the detector side. A single crystal of Fe–Al phase D was polished on both sides down to ~20 μm thickness and loaded along with a ruby sphere for pressure measurements. Helium was used as pressure medium using the COMPRES-GSECARS gas loading system at the APS (Rivers et al., 2008). To control the pressure increment in small and consistent steps of ~0.5 GPa, the four bolts on the diamond-anvil cell were attached to a gearbox. An online ruby fluorescence system was setup to measure the *in situ* pressure while remotely increasing pressure to ensure small and consistent pressure increments. Run#1 was carried out to ~40 GPa, and lattice parameters were refined using the program UnitCell (Holland and Redfern, 1997).

The setup for compression run#2 was similar to run#1, except two single crystals of phase D in different orientations were double polished and loaded together into the pressure chamber, providing a wider coverage of reflections and therefore better constraints on lattice parameters. The cell was gas loaded with neon as pressure medium by using the same setup as in run#1. X-ray diffraction experiments were carried out up to 82 GPa on the 16-IDD beamline using a CCD detector. At the first pressure, omega step-scans ±20° were performed with a rotation of one degree per step and exposure time 2 s/step. The step-scan images were used to create an orientation matrix for indexing the peak positions in the subsequent pressures. Subsequently, wide angle scans were performed with rotating angle of ±12.5° about the X-ray beam with exposure times of 25 s. The lattice parameters of phase D in run#2 were refined by combining all the reflections from two crystals using the software packages GSE_ADA (Dera, 2007a) and RSV (Dera, 2007b). For comparison, the lattice parameters were also fitted using the program UnitCell (Holland and Redfern, 1997), and the resulting lattice parameters from these two software packages were identical within reported uncertainty.

3. Results

3.1. Electronic spin transition of Fe³⁺ in phase D

Fig. 2a shows the Fe-Kβ X-ray emission spectra of the Fe–Al phase D at various pressures up to 94 GPa. Presence of the Kβ' peak at ~7045 eV at ambient pressure is indicative of Fe³⁺ in the high spin (HS) state originating from 3p–3d electronic exchange interaction (e.g. Lin et al., 2010). The gradual disappearance of the Kβ' peak signifies a pressure-induced HS to LS transition of Fe³⁺. The intensity of the Kβ' peak begins decreasing at ~40 GPa, and eventually disappears above ~65 GPa. The low-spin fraction (n) as

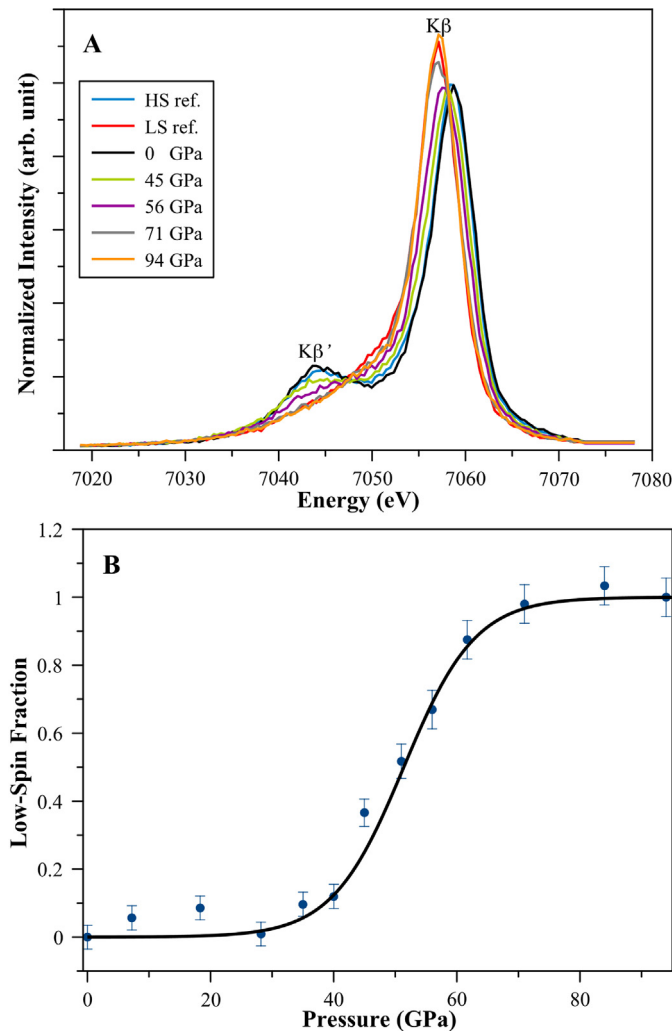


Fig. 2. (a) X-ray emission spectra of Fe–Al phase D at various pressures up to 94 GPa. The blue curve was measured on hematite at room-pressure and served as the high-spin Fe reference. The red curve was measured on $(\text{Mg}_{0.75}\text{Fe}_{0.25})\text{O}$ at 90 GPa (Mao et al., 2011) and served as the low-spin reference. (b) The low-spin fraction (n) as a function of pressure, $n(P)$, was calculated by comparing the integrals of the absolute values of the difference spectra (IAD methods) (Vankó et al., 2006). (For interpretation of the references to color in this figure legend, the reader is referred to the web version of this article.)

a function of pressure, $n(P)$, was calculated by comparing the integrals of the absolute values of the difference spectra (IAD methods) (Vankó et al., 2006), shown in Fig. 2b. Our results indicate that the octahedral- Fe^{3+} spin-transition interval in phase D is 40–65 GPa.

The observed Fe^{3+} spin-transition interval in phase D is similar to the HS–LS transition pressure interval of Fe^{2+} in $(\text{Mg},\text{Fe})\text{O}$ at 40–70 GPa (e.g. Badro et al., 2003; Lin et al., 2005). Catalli et al. (2011) reported a sharper and higher-pressure HS–LS transition of Fe^{3+} in Fe–Al silicate perovskite at 70–83 GPa, in contrast to what Catalli et al. (2010) observed in Al-free Fe-perovskite where Fe^{3+} in the B site is completely low spin by ~ 60 GPa and Fe^{3+} in the A site remains HS to pressures in excess of 130 GPa. Using synchrotron Mössbauer spectroscopy, Lin et al. (2012) observed a spin transition of Fe^{3+} on the B site between 13 and 24 GPa and a constant high-spin state of Fe^{3+} on the A site up to 120 GPa, consistent with theoretical calculations by Hsu et al. (2011). Further calculations by Hsu et al. (2012) reported that Fe–Al perovskite behaves similar to Al-free perovskite, finding that Fe^{3+} undergoes a spin transition at 40–70 GPa on the B site, whereas Fe^{3+} on the A site remains high spin throughout the lower-mantle pressure range. Therefore, the pressure interval of the Fe^{3+} HS–LS

Table 2
Variation of lattice parameters with pressure for Fe–Al phase D.

Pressure (GPa)	a (Å)	c (Å)	V (Å ³)	c/a	Run#
Ambient	4.7964(1)	4.3224(4)	86.116(7)	0.90116	
1.70(±0.1)	4.7833(9)	4.3026(20)	85.25(1)	0.89952	2
3.13	4.7754(9)	4.2796(18)	84.52(1)	0.89618	2
3.90	4.7668(7)	4.2755(10)	84.13(1)	0.89694	1
4.45	4.7617(7)	4.2698(10)	83.84(1)	0.89670	1
4.97	4.7552(6)	4.2631(13)	83.48(1)	0.89650	2
5.18	4.7543(7)	4.2649(10)	83.49(1)	0.89707	1
5.89	4.7484(7)	4.2589(10)	83.16(1)	0.89691	1
6.79	4.7418(7)	4.2502(10)	82.76(1)	0.89633	1
7.37	4.7431(13)	4.2394(27)	82.59(1)	0.89380	2
7.81	4.7267(7)	4.2361(10)	81.96(1)	0.89621	1
8.90	4.7249(7)	4.2362(10)	81.90(1)	0.89657	1
9.75	4.7200(7)	4.2266(10)	81.55(1)	0.89547	1
10.41	4.7173(39)	4.2167(81)	81.14(4)	0.89457	2
10.74	4.7147(7)	4.2169(10)	81.18(1)	0.89440	1
11.87	4.7085(7)	4.2074(10)	80.78(1)	0.89357	1
12.92	4.7044(7)	4.1971(10)	80.44(1)	0.89217	1
13.58	4.6964(7)	4.1867(14)	79.97(1)	0.89147	2
14.08	4.6952(7)	4.1897(10)	79.98(1)	0.89233	1
14.91	4.6905(7)	4.1838(10)	79.72(1)	0.89198	1
15.91	4.6825(6)	4.1734(10)	79.25(1)	0.89128	1
16.75	4.6792(6)	4.1683(10)	79.04(1)	0.89080	1
17.79	4.6727(9)	4.1564(16)	78.59(1)	0.88950	2
17.96	4.6687(6)	4.1639(10)	78.60(1)	0.89188	1
18.98	4.6625(6)	4.1546(10)	78.22(1)	0.89106	1
19.90	4.6571(6)	4.1530(10)	78.01(1)	0.89175	1
20.85	5.6520(6)	4.1461(10)	77.71(1)	0.89126	1
21.89	4.6466(6)	4.1393(10)	77.40(1)	0.89084	1
22.47	4.6442(7)	4.1285(14)	77.12(1)	0.88896	2
22.94	4.6379(6)	4.1393(10)	77.03(1)	0.89157	1
23.87	4.6344(6)	4.1299(10)	76.82(1)	0.89113	1
24.82	4.6297(6)	4.1244(10)	76.56(1)	0.89087	1
25.92	4.6260(6)	4.1162(10)	76.28(1)	0.88980	1
26.88	4.6233(6)	4.1112(10)	76.10(1)	0.88924	1
27.91	4.6164(6)	4.1042(10)	75.75(1)	0.88905	1
29.20	4.6108(6)	4.0985(10)	75.46(1)	0.88889	1
29.81	4.6059(6)	4.0975(10)	75.28(1)	0.88962	1
30.85	4.6003(11)	4.0816(23)	74.81(1)	0.88725	2
30.95	4.6031(6)	4.0921(10)	75.09(1)	0.88898	1
31.78	4.5947(6)	4.0950(10)	74.87(1)	0.89125	1
32.80	4.5917(6)	4.0851(9)	74.59(1)	0.88966	1
33.90	4.5898(6)	4.0781(9)	74.40(1)	0.88850	1
34.83	4.5848(6)	4.0789(9)	74.25(1)	0.88965	1
35.75	4.5833(6)	4.0709(9)	74.06(1)	0.88821	1
35.76	4.5887(28)	4.0705(62)	74.23(3)	0.88708	2
36.84	4.5776(6)	4.0689(9)	73.84(1)	0.88887	1
37.49	4.5737(6)	4.0680(9)	73.70(1)	0.88943	1
39.00	4.5698(6)	4.0567(9)	73.37(1)	0.88773	1
40.20	4.5599(13)	4.0269(28)	72.51(1)	0.88309	2
44.35	4.5376(14)	4.0079(28)	71.47(1)	0.88326	2
48.98	4.5191(12)	3.9896(25)	70.56(1)	0.88283	2
52.78	4.5029(13)	3.9644(30)	69.61(1)	0.88040	2
55.44	4.4929(13)	3.9539(26)	69.12(1)	0.88003	2
58.66	4.4772(13)	3.9461(28)	68.50(1)	0.88138	2
61.51	4.4658(16)	3.9391(34)	68.31(2)	0.88206	2
64.09	4.4537(19)	3.9369(38)	67.63(2)	0.88396	2
65.50	4.4472(12)	3.9228(23)	67.19(1)	0.88207	2
69.60	4.4289(14)	3.9054(19)	66.34(1)	0.88178	2
71.35	4.4295(14)	3.8991(30)	66.25(1)	0.88026	2
74.49	4.4163(13)	3.9043(27)	65.95(1)	0.88408	2
79.07	4.4056(32)	3.8825(68)	65.26(3)	0.88126	2
81.67	4.3944(12)	3.8855(23)	64.98(1)	0.88420	2

transition in phase D is similar to Fe^{2+} in $(\text{Mg},\text{Fe})\text{O}$ and similar to octahedral Fe^{3+} in silicate perovskite (Catalli et al., 2010; Hsu et al., 2012) but occurs at higher pressure than Fe^{3+} in silicate perovskite as reported by Lin et al. (2012).

3.2. Equation of state of Fe–Al phase D

Compression data for Fe–Al phase D through the HS-to-LS transition are listed in Table 2 and plotted in Fig. 3. A discontinuity in the compression curve occurs at ~ 40 GPa, which coincides

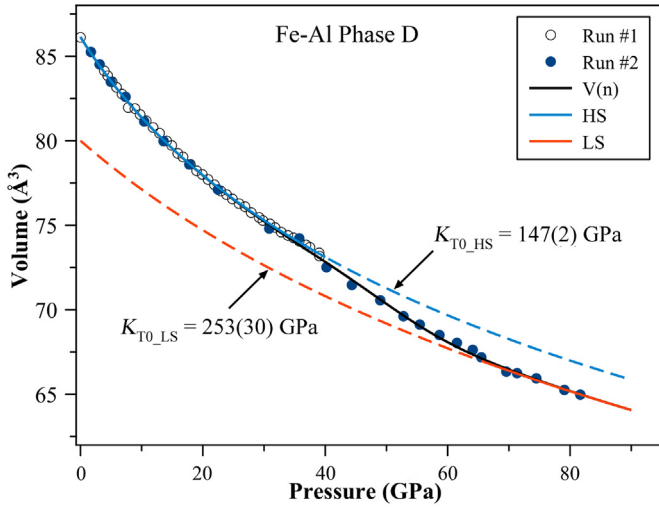


Fig. 3. Volume compressibility of Fe–Al phase D. The blue curve, dashed where extrapolated, represents the fitted equation of state for high-spin phase D. The red curve represents the equation of state for low-spin phase D. The black curve is the complete spin-transition equation of state fitted using the procedure of Wentzcovitch et al. (2009). (For interpretation of the references to color in this figure legend, the reader is referred to the web version of this article.)

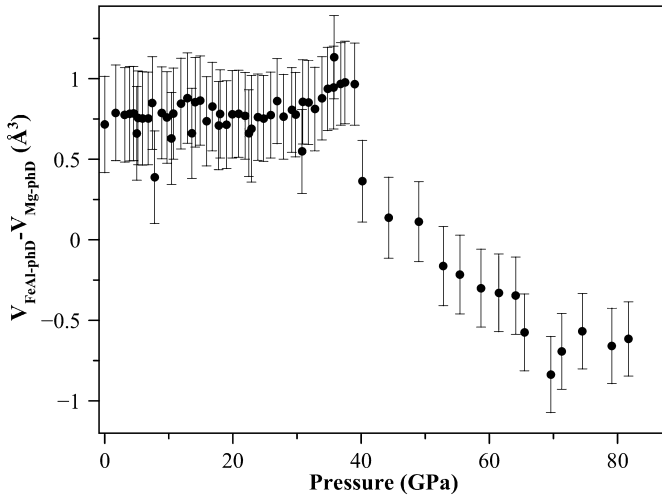


Fig. 4. The difference in volume between Fe–Al phase D (this study) and the volume of pure-Mg phase D, calculated from the equation of state of Hushur et al. (2011). Discontinuities at ~40 and at 65 GPa further constrain the Fe³⁺ spin-transition region. (For interpretation of the references to color in this figure legend, the reader is referred to the web version of this article.)

with the onset of the HS-to-LS transition of Fe³⁺ interpreted by XES, but also at the pressure of a predicted hydrogen-bond symmetrization (Tsuchiya et al., 2005). Therefore, the volume changes in Fe–Al phase D at around 40 GPa are potentially influenced by both hydrogen-bond symmetrization and the Fe-spin transition simultaneously. A second discontinuity in the compression curve occurs at ~65 GPa, likely corresponding to completion of the Fe³⁺ spin transition. To further examine HS–LS transition pressure range in Fe–Al phase D, we calculated the difference between measured unit-cell volumes in this experiment ($V_{\text{FeAl-phD}}$) and those calculated from the equation of state of pure-Mg phase D ($V_{\text{Mg-phD}}$) from Hushur et al. (2011). The resulting ΔV data, shown in Fig. 4, show discontinuities at around 40 GPa and 65 GPa, corresponding exactly to the HS–LS transition interval interpreted from our XES spectra (Fig. 2).

For the purpose of deriving a spin-transition equation of state covering the entire experimental pressure range, we divided the

compression data into three regions: ambient to 40 GPa for the HS state, 40–65 GPa for the mixed-spin state, and above 65 GPa for the LS state. Below 40 GPa, run#1 agrees very well with run#2, indicating that these two datasets are compatible and can be combined into one dataset (Table 1). We obtained a 3rd-order Birch–Murnaghan equation of state for HS Fe–Al phase D yielding $K_{T0_HS} = 147(2)$ GPa, $K'_{T0_HS} = 6.3(3)$ and $V_{0_HS} = 86.14(3)$ Å³. The fitted V_{0_HS} for Fe–Al phase D is equal within error to our experimental value of $V_0 = 86.116(7)$ Å³.

The six volume–pressure data within the LS range were similarly fitted to a 3rd-order Birch–Murnaghan equation of state by minimizing the sum-of-squares misfit over the parameter space, yielding an LS equation of state for Fe–Al phase D with $K_{T0_LS} = 253(30)$ GPa, $K'_{T0} = 4.2(3)$ and $V_{0_LS} = 80(1)$ Å³. To model the elastic properties of phase D through the spin transition, we followed the method of Wentzcovitch et al. (2009) using the resulting K_{T0_HS} , V_{0_HS} , K_{T0_LS} , V_{0_LS} , and the low-spin fraction as a function of pressure, $n(P)$, to model variation of the volume and bulk modulus as a function of n using Eqs. (1)–(3):

$$V(n) = nV_{LS}(P, T) + (1 - n)V_{HS}(P, T) \quad (1)$$

$$\frac{V(n)}{K(n)} = n \frac{V_{LS}}{K_{LS}} + (1 - n) \frac{V_{HS}}{K_{HS}} - (V_{LS} - V_{HS}) \frac{\partial n}{\partial P} \Big|_T \quad (2)$$

In Eqs. (1)–(2), $n(P, T)$ is the LS fraction defined as:

$$n = \frac{1}{1 + \exp(\Delta G(P, T) * / T)} \quad (3)$$

where $\Delta G(P, T) *$ is the difference of the Gibbs free energy between the LS and HS states (e.g. Mao et al., 2011). This model has been used successfully to derive the low-spin fraction of Fe²⁺ in lower-mantle ferropervskite using experimentally measured thermal equation-of-state data (Mao et al., 2011).

The derived low-spin fraction as a function of pressure is shown fitted to the experimental data in Fig. 2b, which was used to calculate $V(n)$ and $K(n)$ using Eqs. (1)–(2). In Fig. 3, the volume-compression data are plotted along with the HS, LS, and complete spin-transition equations of state. The region of largest misfit occurs right around the transition at ~40 GPa, possibly due to the fact that we are only modeling the volume change as a function of the low-spin fraction and not incorporating possible volume effects due to a proposed hydrogen bond symmetrization. However, the data between 40 and 45 GPa fall slightly below the fitted equation of state, indicating a more abrupt softening than modeled by our spin-transition equation of state in contrast to the stiffening effect of hydrogen-bond symmetrization predicted by Tsuchiya et al. (2005) and the discontinuity observed at ~40 GPa in Mg-phase D by Hushur et al. (2011).

Our results show that the electronic spin transition of Fe³⁺ in phase D causes a similar volume contraction to the HS–LS transition in (Mg,Fe)O (e.g. Lin et al., 2005). Variation of the bulk modulus as a function of LS fraction is plotted in Fig. 5a, showing pronounced elastic softening within the spin-transition region between 40 and 65 GPa. The magnitude of bulk modulus softening reaches ~35% at 50 GPa. The variation of $K(n)$ with pressures shows a recovery of the bulk modulus to values extrapolated from the HS state by about 70 GPa. For comparison, we also plotted the bulk modulus of pure-Mg and Fe–Al-bearing silicate perovskite from Boffa Ballaran et al. (2012). Remarkably, above about 65 GPa Fe–Al phase D in the LS state has a similar bulk modulus to silicate perovskite within error, despite containing nearly 10 wt.% H₂O.

In Fig. 5b, the 300 K bulk sound velocity, $V_\phi = (K/\rho)^{1/2}$, is shown for Fe–Al phase D in comparison with silicate perovskite. The velocity contrast between Fe–Al phase D and Fe–Al silicate perovskite reaches a minimum of about 10% at ~50 GPa in the mid-part of the HS–LS transition, but above ~70 GPa the bulk

sound velocity of Fe–Al phase D is actually higher than silicate perovskite by nearly 10%. Therefore, layers of compositional het-

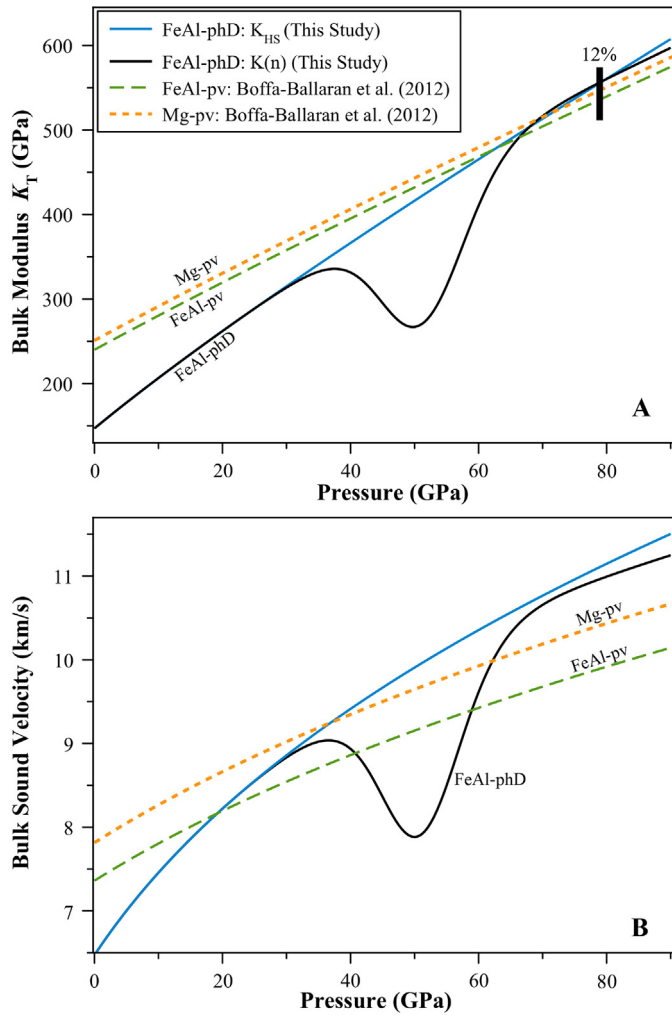


Fig. 5. (a) Variation of the bulk modulus (K) for Fe–Al phase D in the HS state (solid blue curve), and for our model where the fraction of low-spin Fe^{3+} varies with pressure according to the XES measurements (solid black curve). For comparison, we also plot K of pure-Mg and Al–Fe-bearing silicate perovskite from Boffa Ballaran et al. (2012). The black bar represents 12% uncertainty in the low-spin bulk modulus of phase D, $K_{T0,LS} = 253(30)$ GPa, and illustrates that perovskite bulk moduli fall within that uncertainty. (b) Plot of the calculated bulk-sound velocity for phase D compared with silicate perovskite. (For interpretation of the references to color in this figure legend, the reader is referred to the web version of this article.)

Table 3

Equation of state parameters for phase D of various compositions from this and other studies.

Formula	V_0 (\AA^3)	ρ_0 (g/cm^3) [†]	K_0 (GPa)	K'_0	P_{max}	Method*	Reference
Mg phase D							
$Mg_{1.11}Si_{1.6}H_{3.6}O_6$	85.66(1)	3.33	166(3)	4.1(3)	30 GPa	XRD	Frost and Fei (1999)
$Mg_{1.02}Si_{1.73}H_{3.03}O_6$	85.43	3.34	130(1)	7.4(1)	46 GPa	XRD	Shinmei et al. (2008)
$Mg_{1.0}Si_{1.7}H_{3.0}O_6$	85.1(2)	3.34	168(9)	4.3(5)	30 GPa	XRD	Hushur et al. (2011)
	85.4(3)	3.33	150(9)	5.5(4)	55.8 GPa	XRD	
$Mg_{1.02}Si_{1.71}H_{3.12}O_6$	84.74(2)	3.37	175(15)		Ambient	BS	Liu et al. (2004)
$Mg_{1.1}Si_{1.9}H_{2.4}O_6$	85.6(2)	3.46	154.8(3.2)		Ambient	BS	Rosa et al. (2012)
Al–Fe-bearing phase D							
$Mg_{0.89}Fe_{0.14}Al_{0.25}Si_{1.56}H_{2.93}O_6$	86.10(5)	3.45	136.5(3.3)	6.3(3)	30.5 GPa	XRD	Litasov et al. (2007)
$Mg_{0.99}Fe_{0.12}Al_{0.09}Si_{1.75}H_{2.51}O_6$	85.32(2)	3.52	141.5(3.0)	6.2(4)	20.6 GPa	XRD	Litasov et al. (2008)
$Mg_{1.0}Fe_{0.11}Al_{0.03}Si_{1.9}H_{2.5}O_6$	85.1(2)	3.57	158.4(3.9)		Ambient	BS	Rosa et al. (2012)
$MgFe_{0.15}^{3+}Al_{0.32}Si_{1.5}H_{2.6}O_6$	86.14(3)	3.51	147(2)	6.3(3)	40 GPa	XRD	This study
Low-spin phase D	80.00	3.78	253(30)	4.2(3)	65–82 GPa	XRD	This study

* XRD: X-ray diffraction; BS: Brillouin scattering.

† Density was calculated using the formula weight and V_0 .

erogeneity in slabs containing 10% Fe–Al phase D may be capable of producing bulk sound velocity contrast on the order of 1%. Implications for interpreting small-scale heterogeneities in the mid-lower mantle are further discussed in Section 3.4.

3.3. Effects of Fe and Al on bulk and axial compressibility of phase D

The bulk modulus of HS Fe–Al phase D obtained in this study, $K_{T0} = 147(2)$ GPa, is about 5% lower than a result from Brillouin scattering on Fe–Al phase D by Rosa et al. (2012), who obtained $K_{S0} = 158(4)$ GPa. The iron and hydrogen content of our sample is comparable to the study of Rosa et al. (2012) (Table 3). However, our sample contains about 0.3 Al per formula unit, about one order of magnitude more Al than the sample from Rosa et al. (2012), suggesting that the additional Al may have slightly reduced the bulk modulus. There are other compositional factors to consider; for example, the $(Mg + Fe)/Si$ ratio of the sample from Rosa et al. (2012) was about 0.58, compared with 0.76 in our sample (Table 3).

Our results for the bulk modulus of HS Fe–Al phase D are about 7% higher than the sample of Fe–Al phase D studied by Litasov et al. (2007), who reported $K_{T0} = 136.5(3.3)$ GPa and $K' = 6.3(3)$ (Table 3). Compared with our sample, the composition from Litasov et al. (2007) had more hydrogen, with 2.9 H per formula unit and a lower $(Mg + Fe)/Si$ ratio of 0.66, compared with our sample having 2.6 H per formula unit and $(Mg + Fe)/Si$ of about 0.76 (Table 3). Litasov et al. (2008) reported $K_{T0} = 141(3)$ GPa with $K' = 6.2(4)$ for a phase D with 2.5 H, 0.09 Al, and 0.12 Fe (per formula unit) and a Mg/Si ratio of 0.57 (Table 3). The fitted K' from this study for high-spin Fe–Al phase D, $K' = 6.3(3)$, is identical to the fitted K' from Litasov et al. (2007) and Litasov et al. (2008), thus we may directly compare values of the bulk moduli. However, at present there are too few studies and too many compositional factors (including Fe-content, Al-content, H-content, $(Mg + Fe)/Si$, and $Fe^{3+}/\sum Fe$ ratios) to draw any definitive crystal chemical trends for variation of phase D elastic properties with composition.

Compared with Mg-phase D (e.g. Hushur et al., 2011), the Fe–Al phase D in this study has a slightly shorter c -axis and slightly longer a -axis. The layered structure of phase D results in anisotropic compression of the a - and c -axes, shown in Fig. 6a. The axial incompressibility of the a -axis (β_a) in this Al–Fe-phase D is about half that of β_c , similar to results on Mg-phase D. The volume discontinuity caused by the spin transition appears to result almost entirely from shortening of the c -axis, as observed at ~ 40 GPa in Fig. 6a.

On compression, the c/a ratio of pure-Mg and Fe–Al phase D decreases with pressure but eventually becomes constant (Fig. 6b).

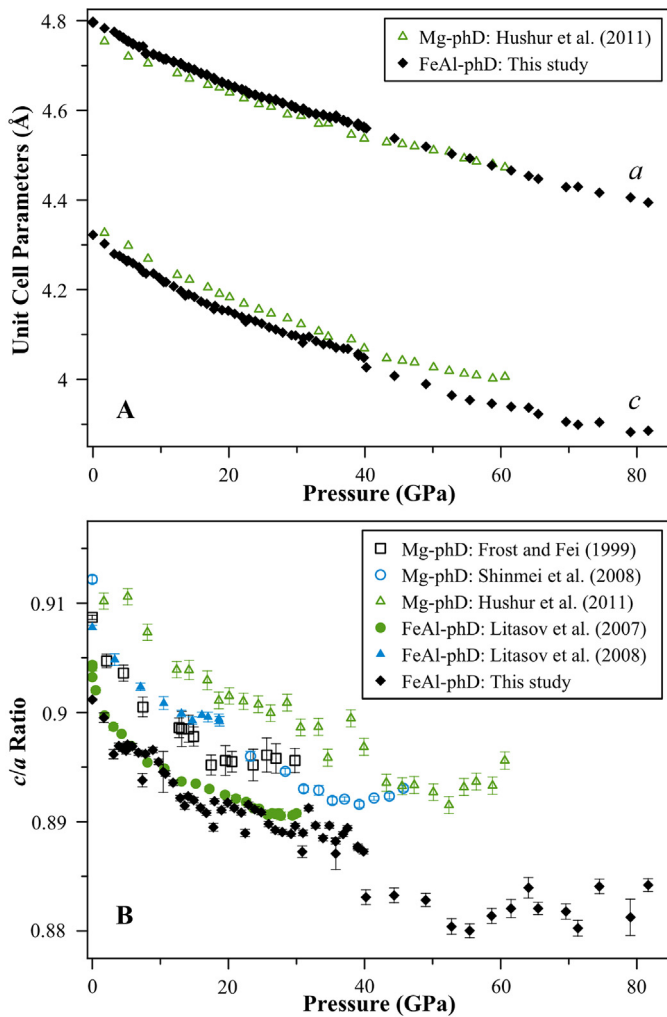


Fig. 6. (a) Variation of the lattice parameters of Fe–Al phase D from this study (filled diamonds) and pure-Mg phase D (open triangles). (b) Variation of the c/a ratio for Fe–Al phase D (filled symbols) and pure-Mg phase D (open symbols).

The pressure above which c/a is constant varies drastically between studies, ranging from ~ 20 GPa (Frost and Fei, 1999) to ~ 40 GPa (Hushur et al., 2011) for pure-Mg phase D. In the current study, c/a for Fe–Al phase D becomes constant above 40 GPa accompanied by a sharp discontinuity in the trend (Fig. 6b). The cause of this behavior is not agreed upon. Hushur et al. (2011) speculated that c/a becomes constant for the symmetrically hydrogen bonded phase predicted by Tsuchiya et al. (2005). However, a high-pressure FTIR study up to 42 GPa by Shieh et al. (2009) shows no major changes other than gradual shifts in the OH-stretching modes with pressure. The fact that c/a ceases to decrease above 40 for pure-Mg phase D (Hushur et al., 2011), similar to this study, suggests that the behavior may not be related to the spin transition of Fe. Similar behavior in c/a has been observed for brucite, $\text{Mg}(\text{OH})_2$ (e.g. Duffy et al., 1995). Structure refinements of phase D over this pressure range will be required to determine what causes the observed change in compression mechanism.

3.4. Implications for small-scale heterogeneity in the mid-lower mantle

Due to the spin transition of Fe, the presence of Fe–Al-rich phase D in subducted slabs entering the lower mantle may be detected with high-spatial resolution seismic methods. Short-period seismic studies of the mid-lower mantle beneath the Pacific rim have detected kilometer-scale heterogeneities at various depths

around 1500 km (e.g. Kaneshima and Helffrich, 1998, 1999, 2009, 2010). Characterized by late arrivals from S-to-P converted phases, the depth of seismic scatterers ranges from about 1100–1800 km, although the most prominent scatterers occur at a depth of 1500 km (Kaneshima and Helffrich, 2010). Scattered wave amplitudes range from 1 to 10% of the direct P waves, and are associated with slow S-wave velocity anomalies on the order of 1–4% (Kaneshima and Helffrich, 2010). In some areas, such anomalies have been modeled as thin, dipping layers <10 km thick and having low S-wave velocity but high density (Kaneshima and Helffrich, 1999; Niu et al., 2003).

Because of their association with subducted oceanic crust, the fine-scale heterogeneities in the mid-lower mantle have been attributed to silica-saturated basalts producing free-silica phases which survive into the mid-lower mantle (e.g. Bina, 2010). Although free-silica phases in MORB would be seismically fast compared with the surrounding basaltic assemblage, the second-order phase transition of SiO_2 from stishovite to the CaCl_2 structure could produce a softening with S-wave anomalies large enough to be detectable seismically in the lower mantle (e.g. Carpenter et al., 2000; Karki et al., 2001). A minimum in the SiO_2 transition soft mode is expected to occur at ~ 1500 km, which is the depth corresponding to greatest scattering potential, but recovery of velocities to ambient levels would cause the heterogeneities to disappear below about 2000 km, consistent with the observations (e.g. Kaneshima and Helffrich, 2009). Velocity anomalies in eclogite can also be attributed to low S-wave velocities associated with Al-rich stishovite (Lakshtanov et al., 2007). Preservation of free-silica within basaltic layers in the lower mantle could be explained as armored relics, cut off from reaction with the surrounding mantle by very slow diffusion rates (Bina, 2010).

Three lines of evidence establish that the spin-transition interval of Fe^{3+} in phase D at 40–65 GPa overlaps with the depth range of observed mid-lower mantle seismic scatterers: analysis of high-pressure Fe-K β X-ray emission spectra, discontinuities in the volume–compression curve, and discontinuities in $\Delta V(P)$ between Fe–Al phase D and pure-Mg phase D. Onset of the spin transition occurs at the same pressure as the predicted hydrogen-bond symmetrization (Tsuchiya et al., 2005). However, the pronounced softening of the bulk modulus by 35% at 50 GPa (compared with HS phase D) is not consistent with the predicted increase of 20% in the incompressibility of symmetrically-hydrogen bonded phase D (Tsuchiya et al., 2005). If both stiffening of the bulk modulus by 20% due to hydrogen-bond symmetrization, and softening due to the spin transition were occurring simultaneously, a less pronounced volume discontinuity might be expected. At present, we believe there is insufficient experimental evidence to suggest that hydrogen-bond symmetrization has occurred in Fe–Al phase D.

Although bulk-elastic softening is observed during the transition, similar to Fe-spin transitions in $(\text{Mg,Fe})\text{O}$ (Lin et al., 2005; Crowhurst et al., 2008; Marquardt et al., 2009) and silicate perovskite (Hsu et al., 2011), the recovered low-spin phase D above ~ 65 GPa exhibits an incompressibility comparable to silicate perovskite at lower-mantle pressures. During the HS–LS transition, the bulk sound velocity of Fe–Al phase D reaches a minimum at ~ 50 GPa and is nearly 10% slower than silicate perovskite, but recovers and becomes 10% faster than silicate perovskite above 70 GPa. The stability field of Fe–Al rich DHMS requires further study, but if Fe–Al phase D remains stable into the deep lower mantle, its elastic properties suggest that it could provide an alternative explanation for small-scale seismic scatterers observed in subducted slabs at 1100–1800 km depth. As a potential carrier of H_2O into the lower mantle, Fe–Al phase D should be considered in geochemical and geodynamic models of Earth's deep water cycle.

4. Conclusions

Our observations of bulk-elastic softening in Fe–Al phase D from 40–65 GPa provide an alternative explanation for the small-scale seismic scatterers in the mid-lower mantle. The minimum in bulk-sound velocity contrast between Fe–Al phase D and silicate perovskite, occurring at 50 GPa (~1500 km), coincides with the depth of greatest scattering potential from the small-scale heterogeneities beneath the Pacific rim (e.g. Kaneshima and Helffrich, 2009, 2010). Further, recovery of the velocities in Fe–Al phase D to levels equal to silicate perovskite between 50–70 GPa (1500–2100 km) is also consistent with the depth range where the scattering power of observed heterogeneities diminish (e.g. Kaneshima and Helffrich, 2009, 2010). Although we have inferred softening in the bulk sound velocity from compression experiments, further elasticity measurements are required to determine how the spin transition of Fe in phase D affects S-wave velocities and elastic wave anisotropy. The association of mid-lower mantle seismic scatterers with subducted oceanic crust, if explained by the presence of Fe–Al phase D, would imply that components from deeply-subducted hydrous sediments with Fe–Al rich compositions, such as mudstones and shales, are being carried into the lower mantle.

Acknowledgements

This research was supported by the Carnegie/DOE Alliance Center (CDAC) and by US NSF grants EAR-0748707 (CAREER) to S.D.J. and by EAR-1056670 and EAR-1053446 to J.F.L. Additional support was provided by the David and Lucile Packard Foundation to S.D.J. Portions of this work were performed at HPCAT (Sector 16), Advanced Photon Source (APS), Argonne National Laboratory. HPCAT operations are supported by DOE-NNSA under Award No. DE-NA0001974 and DOE-BES under Award No. DE-FG02-99ER45775, with partial instrumentation funding by NSF. Use of the COMPRES-GSECARS gas loading system was supported by COMPRES under NSF Cooperative Agreement EAR 11-57758 and by GSECARS through NSF grant EAR-1128799 and DOE grant DE-FG02-94ER14466. Use of the Advanced Photon Source was supported by the U.S. Department of Energy, Office of Science, Office of Basic Energy Sciences, Contract No. DE-AC02-06CH11357.

References

- Angel, R.J., Frost, D.J., Ross, N.L., Hemley, R., 2001. Stabilities and equations of state of dense hydrous magnesium silicates. *Phys. Earth Planet. Inter.* 127, 181–196.
- Badro, J., Fiquet, G., Guyot, F., Rueff, J., Struzhkin, V., 2003. Iron partitioning in Earth's mantle: Toward a deep lower mantle discontinuity. *Science* 300, 789–791.
- Badro, J., Rueff, J.P., Vankó, G., Monaco, G., Fiquet, G., Guyot, F., 2004. Electronic transitions in perovskite: possible nonconvecting layers in the lower mantle. *Science* 305, 383–386.
- Bina, C.R., 2010. Scale limits of free-silica seismic scatterers in the lower mantle. *Phys. Earth Planet. Inter.* 183, 110–114.
- Boffa Ballaran, T., Frost, D.J., Miyajima, N., Heidelbach, F., 2010. The structure of a super-aluminous version of the dense hydrous-magnesium silicate phase D. *Am. Mineral.* 95, 1113–1116.
- Boffa Ballaran, T., Kurnosov, A., Glazyrin, K., Frost, D.J., Merlini, M., Hanfland, M., Caracas, R., 2012. Effect of chemistry on the compressibility of silicate perovskite in the lower mantle. *Earth Planet. Sci. Lett.* 333–334, 181–190.
- Carpenter, M.A., Hemley, R.J., Mao, H.K., 2000. High-pressure elasticity of stishovite and the $P4(2)/mmm-Pnmm$ phase transition. *J. Geophys. Res.* 105, 10807–10816.
- Catalli, K., Shim, S.-H., Prakapenka, V.B., Zhao, J., Sturhahn, W., Chow, P., Xiao, Y., Liu, H., Cynn, H., Evans, W.J., 2010. Spin state of ferric iron in $MgSiO_3$ perovskite and its effect on elastic properties. *Earth Planet. Sci. Lett.* 289, 68–75.
- Catalli, K., Shim, S.-H., Dera, P., Prakapenka, V.B., Zhao, J., Sturhahn, W., Chow, P., Xiao, Y., Cynn, H., Evans, W.J., 2011. Effects of the Fe^{3+} spin transition on the properties of aluminous perovskite – new insights for lower-mantle seismic heterogeneities. *Earth Planet. Sci. Lett.* 310, 293–302.
- Crowhurst, J.C., Brown, J.M., Goncharov, A.F., Jacobsen, S.D., 2008. Elasticity of $(Mg,Fe)O$ through the spin transition of iron in the lower mantle. *Science* 319, 451–453.
- Dera, P., 2007a. GSE-ADA data analysis program for monochromatic single crystal diffraction with area detector. GeoSoilEnviroCARS, Argonne, Illinois.
- Dera, P., 2007b. RSV reciprocal space viewer program for single crystal data analysis. GeoSoilEnviroCARS, Argonne, Illinois.
- Duffy, T.S., Shu, J., Mao, H.K., Hemley, R.J., 1995. Single-crystal X-ray diffraction of brucite to 14 GPa. *Phys. Chem. Miner.* 22, 277–281.
- Frost, D.J., Fei, Y., 1998. Stability of phase D at high pressure and high temperature. *J. Geophys. Res.* 103, 7463–7474.
- Frost, D.J., Fei, Y., 1999. Static compression of the hydrous magnesium silicate phase D to 30 GPa at room temperature. *Phys. Chem. Miner.* 26, 415–418.
- Frost, D.J., Liebske, C., Langenhorst, F., McCammon, C.A., Trönes, R.G., Rubie, D.C., 2004. Experimental evidence for the existence of iron-rich metal in the Earth's lower mantle. *Nature* 428, 409–412.
- Grocholski, B., Shim, S.H., Sturhahn, W., Zhao, J., 2009. Spin and valence states of iron in $(Mg_{0.8}Fe_{0.2})SiO_3$ perovskite. *Geophys. Res. Lett.* 36, L24303.
- Gütlich, P., Bill, E., Trautwein, A., 2011. Mössbauer Spectroscopy and Transition Metal Chemistry. Springer-Verlag, Berlin. 569 pp.
- Holland, T.J.B., Redfern, S.A.T., 1997. Unit cell refinement from powder diffraction data; the use of regression diagnostics. *Mineral. Mag.* 61, 65–77.
- Hsu, H., Blaha, P., Cococcioni, M., Wentzcovitch, R., 2011. Spin-state crossover and hyperfine interactions of ferric iron in $MgSiO_3$ perovskite. *Phys. Rev. Lett.* 106, 118501.
- Hsu, H., Yu, Y.G., Wentzcovitch, R.M., 2012. Spin crossover of iron in aluminous $MgSiO_3$ perovskite and post-perovskite. *Earth Planet. Sci. Lett.* 359–360, 34–39.
- Hushur, A., Manghnani, M.H., Smyth, J.R., Williams, Q., Hellebrand, E., Lonappan, D., Ye, Y., Dera, P., Frost, D.J., 2011. Hydrogen bond symmetrization and equation of state of phase D. *J. Geophys. Res.* 116, B06203.
- Irfune, T., Kubo, N., Isshiki, M., Yamasaki, Y., 1998. Phase transformations in serpentine and transportation of water into the lower mantle. *Geophys. Res. Lett.* 25, 203–206.
- Jackson, J.M., Sturhahn, W., Shen, G., Zhao, J., Hu, M.Y., Errandonea, D., Bass, J.D., Fei, Y., 2005. A synchrotron Mössbauer spectroscopy study of $(Mg,Fe)SiO_3$ perovskite up to 120 GPa. *Am. Mineral.* 90, 199–205.
- Kaneshima, S., Helffrich, G., 1998. Detection of lower mantle scatterers northeast of the Marianna subduction zone using short-period array data. *J. Geophys. Res.* 103, 4825–4838.
- Kaneshima, S., Helffrich, G., 1999. Dipping low-velocity layer in the mid-mantle: evidence for geochemical heterogeneity. *Science* 283, 1888–1891.
- Kaneshima, S., Helffrich, G., 2009. Lower mantle scattering profiles and fabric below Pacific subduction zones. *Earth Planet. Sci. Lett.* 282, 234–239.
- Kaneshima, S., Helffrich, G., 2010. Small scale heterogeneity in the mid-lower mantle beneath the circum-Pacific area. *Phys. Earth Planet. Inter.* 183, 91–103.
- Karki, B.B., Stixrude, L., Wentzcovitch, R.M., 2001. High-pressure elastic properties of major materials of Earth's mantle from first principles. *Rev. Geophys.* 39, 507–534.
- Kawakatsu, H., Watada, S., 2007. Seismic evidence for deep-water transportation in the mantle. *Science* 316, 1468–1471.
- Kawamoto, T., 2004. Hydrous phase stability and partial melt chemistry in H_2O -saturated KLB-1 peridotite up to the uppermost lower mantle conditions. *Phys. Earth Planet. Inter.* 143–144, 387–395.
- Komabayashi, T., Omori, S., 2006. Internally consistent thermodynamic data set for dense hydrous magnesium silicates up to 35 GPa, 160 °C: implications for water circulation in the Earth's deep mantle. *Phys. Earth Planet. Inter.* 156, 89–107.
- Lakshtanov, D.L., Sinogeikin, S.V., Litasov, K.D., Prakapenka, V.B., Hellwig, H., Wang, J., Sanches-Valle, C., Perrillat, J.P., Chen, B., Somayazulu, M., Li, J., Ohtani, E., Bass, J.D., 2007. The post-stishovite phase transition in hydrous alumina-bearing SiO_2 in the lower mantle of the Earth. *Proc. Natl. Acad. Sci. USA* 104, 13588–13590.
- Li, J., 2007. Electronic transitions and spin states in the lower mantle. In: Hirose, K., Brodholt, J., Lay, T., Yuen, D. (Eds.), *Post-Perovskite: The Last Mantle Phase Transition*. In: *Geophys. Monogr.*, vol. 174. American Geophysical Union, pp. 47–68.
- Li, J., Struzhkin, V.V., Mao, H.K., Shu, J., Hemley, R.J., Fei, Y., Mysen, B., Dera, P., Prakapenka, V.B., Shen, G., 2004. Electronic spin state of iron in lower mantle perovskite. *Proc. Natl. Acad. Sci. USA* 121, 14027–14030.
- Lin, J.F., Tsuchiya, T., 2008. Spin transition of iron in the Earth's lower mantle. *Phys. Earth Planet. Inter.* 170, 248–259.
- Lin, J.F., Struzhkin, V.V., Jacobsen, S.D., Hu, M.Y., 2005. Spin transition of iron in magnesiowüstite in the Earth's lower mantle. *Nature* 432, 377–380.
- Lin, J.F., Vankó, G., Jacobsen, S.D., Iota, V., Struzhkin, V.V., Prakapenka, V.B., Kuznetsov, A., Yoo, C.S., 2007. Spin transition zone in Earth's lower mantle. *Science* 317, 1740–1743.
- Lin, J.F., Watson, H., Vankó, G., Alp, E., Prakapenka, V.B., Dera, P., Struzhkin, V.V., Kubo, A., Zhao, J., McCammon, C., Evans, W.J., 2008. Intermediate-spin ferrous iron in lowermost mantle post-perovskite and perovskite. *Nat. Geosci.* 1, 688–691.
- Lin, J.F., Mao, Z., Jarrige, I., Xiao, Y., Chow, P., Okuchi, T., Hiraoka, N., Jacobsen, S.D., 2010. Resonant X-ray emission study of the lower-mantle ferroperricline at high pressures. *Am. Mineral.* 95, 1125–1131.

- Lin, J.F., Alp, E.E., Mao, Z., Inoue, T., McCammon, C., Xiao, Y., Chow, P., Zhao, J., 2012. Electronic spin states of ferric and ferrous iron in the lower-mantle silicate perovskite. *Am. Mineral.* 97, 592–597.
- Litasov, K.D., Ohtani, E., 2003. Stability of various hydrous phases in CMAS pyrolite–H₂O system up to 25 GPa. *Phys. Chem. Miner.* 30, 147–156.
- Litasov, K.D., Ohtani, E., Suzuki, A., Funakoshi, K., 2007. The compressibility of Fe- and Al-bearing phase D to 30 GPa. *Phys. Chem. Miner.* 34, 159–167.
- Litasov, K.D., Ohtani, E., Nishihara, Y., Suzuki, A., Funakoshi, K., 2008. Thermal equation of state of Al- and Fe-bearing phase D. *J. Geophys. Res.* 113, B08205.
- Liu, L., Okamoto, K., Yang, Y., Chen, C., 2004. Elasticity of single-crystal Phase D (a dense hydrous magnesium silicate) by Brillouin spectroscopy. *Solid State Commun.* 132, 517–520.
- Luth, R.W., 1995. Is phase A relevant to the Earth's mantle? *Geochim. Cosmochim. Acta* 59, 679–682.
- Mao, H.K., Xu, J., Bell, P.M., 1986. Calibration of the ruby pressure gauge to 800 kbar under quasi-hydrostatic conditions. *J. Geophys. Res.* 91, 4673–4676.
- Mao, Z., Lin, J.-F., Liu, J., Prakapenka, V.B., 2011. Thermal equation of state of lower-mantle ferropericlase across the spin crossover. *Geophys. Res. Lett.* 38, L23308.
- Marquardt, H., Speziale, S., Reichmann, H.J., Frost, D.J., Schilling, F.R., 2009. Single-crystal elasticity of (Mg_{0.9}Fe_{0.1})O to 81 GPa. *Earth Planet. Sci. Lett.* 287, 345–352.
- McCammon, C., 1997. Perovskite as a possible sink for ferric iron in the lower mantle. *Nature* 387, 694–696.
- Niu, F., Kawakatsu, H., Fukao, Y., 2003. Seismic evidence for a chemical heterogeneity in the mantle: A strong and slightly dipping seismic reflector beneath the Mariana subduction zone. *J. Geophys. Res.* 108, <http://dx.doi.org/10.1029/2002JB002384>.
- Ohtani, E., Toma, M., Litasov, K., Kubo, T., Suzuki, A., 2001. Stability of dense hydrous magnesium silicate phases and water storage capacity in the transition zone and lower mantle. *Phys. Earth Planet. Inter.* 124, 105–117.
- Plank, T., Langmuir, C.H., 1998. The chemical composition of subducting sediment and its consequences for the crust and mantle. *Chem. Geol.* 145, 325–394.
- Poli, S., Schmidt, M.W., 2002. Petrology of subducted slabs. *Annu. Rev. Earth Planet. Sci.* 30, 207–235.
- Ringwood, A.E., Major, A., 1967. High-pressure reconnaissance investigations in the system Mg₂SiO₄–MgO–H₂O. *Earth Planet. Sci. Lett.* 2, 130–133.
- Rivers, M., Prakapenka, V.B., Kubo, A., Pullins, C., Holl, C.M., Jacobsen, S.D., 2008. The COMPRES/GSECARS gas-loading system for diamond anvil cells at the advanced photon source. *High Press. Res.* 28, 273–292.
- Rosa, A.D., Sanchez-Valle, C., Ghosh, S., 2012. Elasticity of phase D and implication for the degree of hydration of deep subducted slabs. *Geophys. Res. Lett.* 39, L06304.
- Saikia, A., Boffa Ballaran, T., Frost, D.J., 2009. The effect of Fe and Al substitution on the compressibility of MgSiO₃-perovskite determined through single-crystal X-ray diffraction. *Phys. Earth Planet. Inter.* 173, 153–161.
- Shieh, S.R., Mao, H.K., Hemley, R.J., Ming, L.C., 1998. Decomposition of phase D in the lower mantle and the fate of dense hydrous silicates in subducting slabs. *Earth Planet. Sci. Lett.* 159, 13–23.
- Shieh, S.R., Mao, H.K., Hemley, R.J., Ming, L.C., 2000. In situ X-ray diffraction studies of dense hydrous magnesium silicates at mantle conditions. *Earth Planet. Sci. Lett.* 177, 69–80.
- Shieh, S.R., Duffy, T.S., Liu, Z., Ohtani, E., 2009. High-pressure infrared spectroscopy of the dense hydrous magnesium silicates phase D and phase E. *Phys. Earth Planet. Inter.* 175, 106–114.
- Shinmei, T., Irifune, T., Tsuchiya, J., Funakoshi, K., 2008. Phase transition and compression behavior of phase D up to 46 GPa using multi-anvil apparatus with sintered diamond anvils. *High Press. Res.* 28, 363–373.
- Speziale, S., Milner, A., Lee, V.E., Clark, S.M., Pasternak, M.P., Jeanloz, R., 2005. Iron spin transition in Earth's mantle. *Proc. Natl. Acad. Sci. USA* 102, 17918–17922.
- Speziale, S., Lee, V.E., Clark, S.M., Lin, J.F., 2007. Effects of Fe spin transition on the elasticity of (Mg,Fe)O magnesiowüstites and implications for the seismological properties of the Earth's lower mantle. *J. Geophys. Res.* 112, B10212.
- Stalder, R., Ulmer, P., 2001. Phase relations of a serpentine composition between 5 and 14 GPa: significance of clinohumite and phase E as water carriers into the transition zone. *Contrib. Mineral. Petrol.* 140, 670–679.
- Tsuchiya, J., Tsuchiya, T., Tsuneyuki, S., 2005. First-principles study of hydrogen bond symmetrization of phase D under high pressure. *Am. Mineral.* 90, 44–49.
- Tsuchiya, T., Wentzcovitch, R.M., da Silva, C.R.S., de Gironcoli, S., 2006. Spin transition in magnesiowüstite in Earth's lower mantle. *Phys. Rev. Lett.* 96, 198501.
- Ulmer, P., Trommsdorff, V., 1995. Serpentine stability to mantle depths and subduction-related magmatism. *Science* 268, 858–861.
- Vankó, G., Neisius, T., Molnár, G., Renz, F., Kárpáti, S., Shukla, A., de Groot, F.M.F., 2006. Probing the 3d spin momentum with X-ray emission spectroscopy: the case of molecular-spin transitions. *J. Phys. Chem. B* 110, 11647–11653.
- Vanpeteghem, C.B., Angel, R.J., Ross, N.L., Jacobsen, S.D., Dobson, D.P., Litasov, K.D., Ohtani, E., 2006. *Phys. Earth Planet. Inter.* 155, 96–103.
- Wentzcovitch, R.M., Justo, J.F., Wu, Z., da Silva, C.R.S., Yuen, D.A., Kohlstedt, D., 2009. Anomalous compressibility of ferropericlase throughout the iron spin cross-over. *Proc. Natl. Acad. Sci. USA* 106, 8447–8452.
- Yamamoto, K., Akimoto, S., 1977. The system MgO–SiO₂–H₂O at high pressures and temperatures – stability field for hydroxyl-chondrodite, hydroxyl-clinohumite, and 10-Å phase. *Am. J. Sci.* 277, 288–312.
- Yang, H., Prewitt, C.T., Frost, D.J., 1997. Crystal structure of the dense hydrous magnesium silicate, phase D. *Am. Mineral.* 82, 651–654.